Pump/probe method for fast analysis of visible spectral signatures utilizing asynchronous optical sampling

Paul A. Elzinga, Ronald J. Kneisler, Fred E. Lytle, Yanan Jiang, Galen B. King, and Normand M. Laurendeau

We report the results from a new pump/probe spectrometer for potential use in combustion diagnostics that employs asynchronous optical sampling. The instrument consists of two frequency-doubled mode-locked Nd:YAG lasers operating at slightly different repetition rates, synchronously pumping two dye lasers (rhodamine 6G) to generate the pump and probe beams. The spectral and temporal capabilities of the instrument are examined by obtaining a spectrum and an excited state decay of rhodamine B. The instrument response is shown to be proportional to pump power, probe power, and sample absorptance. Different frequency synthesizers and different modes of triggering are used to study their effect on signal stability.

I. Introduction

Pump/probe methods are commonly employed to measure subnanosecond excited-state processes in liquid and gas phase systems.[1,2] In a previous paper[3] we described the first results from a new pump/probe spectrometer based on asynchronous optical sampling (ASOPS), which avoids many of the experimental difficulties inherent in conventional approaches. This instrument employed a mode-locked frequency-doubled Nd:YAG laser as the pump laser and a synchronously pumped dye laser as the probe laser. We report results from an improved instrument which employs synchronously pumped dye lasers as both the pump and probe lasers. We measure the response of the instrument to changes in laser power and sample concentration and find good agreement with theory. In addition, the spectral and excited state decay properties of rhodamine B are measured demonstrating the improved temporal and spectral capabilities of this instrument.

The current instrument represents a significant step toward the development of a combustion diagnostic for measurement of species concentrations in rapidly quenched high-pressure flames. The ASOPS technique will eventually allow determination of quenching rates and state-to-state relaxation rates in both the upper and lower rotational manifolds of molecules within high-pressure turbulent combustion systems. Ultimately, this will require the utilization of UV pump and probe beams. However, use of visible beams in the current instrument is sufficient to demonstrate the potential of ASOPS.

II. Operating Principles

In conventional pump/probe instruments the pump and probe lasers operate at identical repetition rates, with an optical delay line used to control the relative timing between pulses from the two lasers. In addition, some type of mechanical or electrooptical chopping scheme is generally employed to induce an amplitude modulation on the signal which facilitates the use of synchronous detection.[4–7] In contrast, the ASOPS instrument employs pump and probe lasers operating at slightly different repetition rates. This induces a carefully controlled repetitive phase walk-out of the pump and probe pulse trains. The process is illustrated in Fig. 1(a), which shows the excited-state population produced by several pump pulses and the temporal position of several probe pulses. Each successive probe pulse is delayed in time (relative to the pump pulse train) by a constantly increasing duration which is determined by the beat frequency of the system. Thus each probe pulse samples the excited-state population at a slightly later time than the preceding probe

When this work was done all authors were with Purdue University, West Lafayette, Indiana 47907; Y. Jiang, G. B. King, and N. M. Laurendeau are with the School of Mechanical Engineering, Flame Diagnostics Laboratory, and the other authors are with the Chemistry Department. Paul Elzinga is now with Upjohn Company, Kalamazoo, Michigan 49001.

Received 28 November 1987.
0003-6935/87/194303-07$02.00/0.

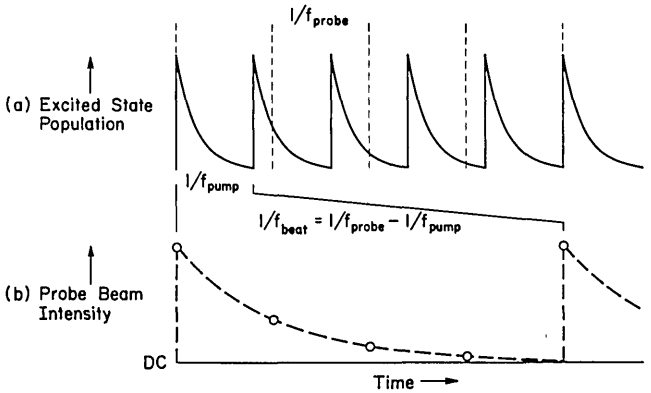

Fig. 1. ASOPS timing diagram showing (a) excited-state population and (b) probe beam intensity. The probe pulses are indicated by the vertical dashed lines.

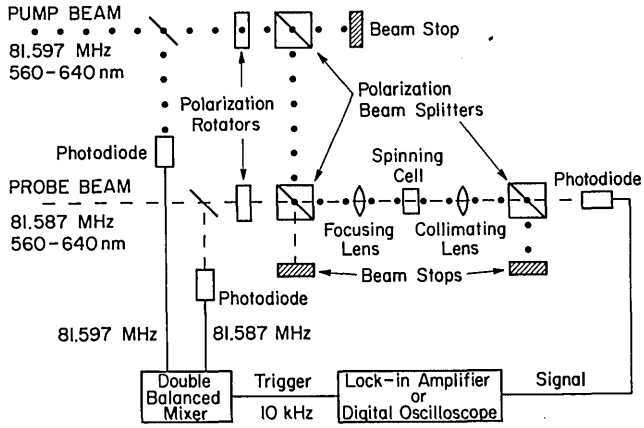

Fig. 2. Block diagram of the ASOPS instrument.

pulse. This is equivalent to varying the optical delay in a conventional instrument. The sampling process repeats itself when the cumulative delay equals the period of the pump laser. Hence any modulation of the probe beam, resulting from the creation and subsequent decay of the excited state, repeats at the beat frequency of the system. Therefore, in contrast to conventional instruments, there is no need to amplitude modulate either beam to employ synchronous detection.

Figure 1(b) illustrates the probe intensity which occurs on stimulated emission from the excited-state population shown in Fig. 1(a). The net effect of the ASOPS technique is that a small amplitude waveform, which is directly related to the fluorescence decay of the species under study, is impressed onto the probe laser intensity. In essence, a time transformation of the excited-state decay is performed with the time scaled by the factor $[f_{pump}/(f_{pump}-f_{probe})]$, where f is the repetition rate of the two lasers. The ASOPS technique is thus an optical analog of the sampling oscilloscope.

III. Equipment and Method

Central to the ASOPS technique is the requirement that the pump and probe lasers operate at slightly different repetition rates. Therefore, the instrument requires two independently mode-locked laser systems. Both the pump and probe beams are derived from Spectra-Physics model 375B dye lasers, which are synchronously pumped by frequency-doubled mode-locked Spectra-Physics series 3000 Nd:YAG lasers. The mode-locking frequencies are generated by two Programmed Test Sources (PTS) model 160 frequency synthesizers operated in a master–slave (i.e., phase-locked) configuration to minimize drift in the beat frequency of the system. Both the pump and probe beams consist of an ~82-MHz train of ~10-ps pulses, tunable (using rhodamine 6G) from 560 to 640 nm. Throughout the center of the tuning range, average powers in excess of 250 mW are obtained using 800–900 mW of pumping power.

A block diagram of the instrument is shown in Fig. 2; Table I summarizes the typical operating conditions employed in temporal studies. The repetition rate of the pump beam determines the free temporal range, which is the maximum time available for a single decay of the excited-state population. The difference in laser periods, which is related to the beat frequency, determines the sampling interval. If the beat frequency is decreased, the sampling interval is also reduced, thereby increasing the temporal resolution. Of course, the number of points necessary to reconstruct the decay also increases and with it the time necessary to collect the data. Note that the PTS frequency synthesizers are accurate to 0.1 Hz. Therefore, the laser repetition rates, and the resulting beat frequencies, are very stable.

Each beam is split as it emerges from the laser. The weaker fraction is used to generate a trigger signal at the beat frequency of the system. This is done by either (1) separately monitoring each beam with fast photodiodes (EG&G FND-100) and electronically mixing the outputs of the photodiodes with a double-balanced mixer (Anzac MD-141) operating in a high-speed gating mode,[8] or (2) generating a cross-correlation of the two pulse trains by combining them in a sum-frequency generating crystal and monitoring the UV output.[9] A typical cross-correlation is shown in Fig. 3. The small pulses are caused by residual doubling of one of the laser beams, while the peak is caused by temporal overlap of the pump and probe pulses in

Table I. Typical Operating Parameters for Temporal Studies

	Pump beam	Probe beam
Wavelength	560–640 nm	560–640 nm
Pulse width	~10 ps	~10 ps
Average power (at cell)	~150 mW	~20 mW
Average power (at photodiode)	—	<20 mW
Repetition rate	81.5870000 MHz	81.5970000 MHz
Beat frequency		10 kHz
Free temporal range		12.2 ns
Sampling interval		1.5 ps
Samples per decay		8200
Collection time (single decay)		100 μs

the crystal. Although not shown, this peak repeats at the beat frequency of the system.

The remaining fractions of both the pump and probe beams pass through polarization rotator–beam splitter combinations which provide a convenient means of varying the power in either beam. In addition, the vertical component of the pump beam is combined with the horizontal component of the probe beam at the second polarization beam splitter. The beams then pass collinearly through a focusing lens, the sample (contained in a spinning cell to minimize thermal lensing problems), and a collimating lens. The beams are then separated by another polarization beam splitter.

For temporal studies, instead of using a polarization beam splitter, the beams are combined with a glass beam splitter (~90% pump transmission, ~10% probe reflection) before passing collinearly through the focusing lens, sample, and collimating lens. The beams are then separated by a narrow bandpass interference filter. Use of the glass beam splitter allows the relative polarization of the pump and probe beams to be set at any desired angle.

The probe beam intensity is monitored by a photodiode (EG&G SGD-100A), the output of which is directed to the detection system. For temporal studies, a digitizing oscilloscope (Hewlett-Packard 54100A), triggered at the beat frequency of the system, was employed. Each point of the oscilloscope signal was the result of 2048 averages. Because of its high sensitivity and large noise-suppression capabilities, a lock-in amplifier (Stanford Research Systems model 510) was used to monitor a single Fourier frequency component of the ASOPS signal for nontemporal studies.

The sample was ~10^{-3}-M rhodamine B (Eastman Kodak, laser grade) in methanol (Fisher Scientific, spectral grade). This molecule was selected because (1) its absorption and emission bands (see Fig. 4)[10] are readily accessible to our dye lasers; (2) its cross sections for absorption and emission are large; and (3) its fluorescence lifetime is short with a quantum yield near unity, thus allowing decay of most of the excited-state population between pump pulses.

IV. Results and Discussion

The pump beam excites molecules of rhodamine B from the ground state S_0 to an upper vibrational level of the first excited S_1, which is followed by instantaneous (on the time scale of this experiment) vibrational relaxation to the lowest vibrational level of S_1. The probe beam can then stimulate emission from this level to an upper vibrational level of S_0, followed again by rapid relaxation to the lowest vibrational level of S_0. The system, therefore, can be analyzed as a simple four-level system with significant population residing only in the lowest vibrational levels of S_0 and S_1. In this case, both the pump and probe transitions can be treated in a Beer's law fashion.[11]

For small gains, the change in the energy of a probe pulse in the absence of rotational diffusion effects is, therefore, given by

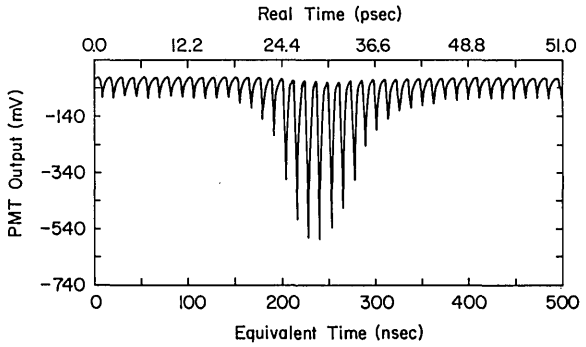

Fig. 3. Cross-correlation of the pump and probe beams.

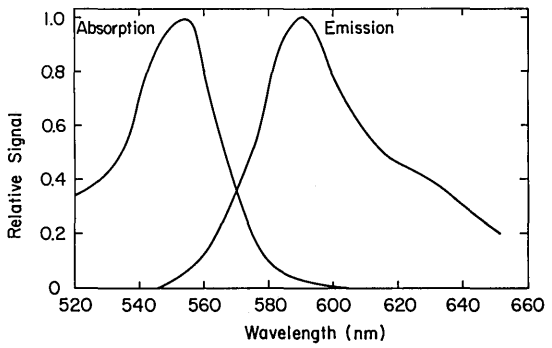

Fig. 4. Normal absorption and fluorescence spectra of rhodamine B.

$$E_{pr}(t) \simeq E_{pr}^0[1 + \sigma_{em} b N_1(t)], \quad (1)$$

where E_{pr}^0 is the probe pulse energy before interaction with the sample, t is the time between the pump and probe pulses, σ_{em} is the cross section for stimulated emission at the probe wavelength, b is the sample path length, and N_1 is the number density of S_1. Since the pump beam is pulsed, N_1 behaves exponentially:

$$N_1(t) = N_1(0) \exp(-t/\tau), \quad (2)$$

where τ is the lifetime of S_1, and $N_1(0)$ is the population of S_1 immediately following the pump pulse. The time-dependent energy of the probe pulse is, therefore, given by

$$E_{pr}(t) = E_{pr}^0[1 + \sigma_{em} b N_1(0) \exp(-t/\tau)]. \quad (3)$$

The lock-in amplifier (LIA), however, measures a time-independent quantity which is proportional to the depth of modulation of the time-dependent signal. Hence

$$V_{LIA} \propto \Delta E_{pr} = E_{pr}(0) - E_{pr}(\Delta t_{pu}), \quad (4)$$

where V_{LIA} is the output voltage of the LIA, ΔE_{pr} is the depth of modulation of the probe beam, $E_{pr}(0)$ is the probe pulse energy immediately following the pump pulse, and Δt_{pu} is the period of the pump laser. If $\Delta t_{pu} \gg \tau$, then $\exp(-\Delta t_{pu}/\tau) \simeq 0$ and $E_{pr}(\Delta t_{pu}) \simeq E_{pr}^0$. Therefore, from Eqs. (3) and (4),

$$V_{LIA} \propto E_{pr}^0 \sigma_{em} b N_1(0). \quad (5)$$

Furthermore, since each absorbed pump photon generates one excited state,

$$N_1(0) = \frac{(E^0_{pu}/h\nu_{pu})(1 - T)_{pu}}{bA_{cs}}, \quad (6)$$

where E^0_{pu} is the energy of a pump pulse before interaction with the sample, ν_{pu} is the optical frequency of the pump beam, A_{cs} is the beam cross-sectional area in the sample, and $(1 - T)_{pu}$ is the sample absorptance at the pump wavelength. Substituting Eq. (6) into Eq. (5), eliminating common terms, and rearranging yield

$$V_{LIA} \propto \left[\frac{\sigma_{em}}{h\nu_{pu}A_{cs}}\right] E^0_{pr}E^0_{pu}(1 - T)_{pu}. \quad (7)$$

Therefore, the LIA signal should respond linearly to changes in probe power, pump power, and sample absorptance.

A. Power Studies

Using the polarization rotators to vary the power in either the pump or probe beam yielded a linear variation in the LIA signal [see Figs. 5(a) and (b)] for pump powers of <150 mW and probe powers of <20 mW (the probe range was limited by the onset of photodiode saturation), as predicted by Eq. (7). For the pump power study, the probe (608 nm) was fixed at ~20 mW, while for the probe power study, the pump (574 nm) was fixed at ~180 mW.

B. Concentration Study

According to Eq. (7), the LIA signal should be proportional to the sample absorptance, which can be calculated from a form of Beer's law as

$$(1 - T)_{pu} = 1 - 10^{-\epsilon_{ab}bC}, \quad (8)$$

where ϵ_{ab} is the molar absorptivity at the pump wavelength and C is the sample concentration.

Unfortunately, the situation is complicated by the fact that the path length b cannot necessarily be equated with the physical width of the cell. This is true because (1) the probe beam is modulated only where the pump and probe beams overlap and (2) the signal is inversely proportional to the cross-sectional area of the beam [see Eq. (7)]. The result is an effective path length which is related to the length of sustained focusing by the probe beam in the presence of the pump beam within the cell. Since relatively tight focusing is currently necessary to generate observable signals, the effective path length in this study was clearly <1 cm (the physical width of the cell), although the exact length is difficult to measure.

Figure 5(c) shows a plot of LIA voltage vs sample absorptance, where the absorptance has been calculated using Eq. (8) from the known molar absorptivity ($\epsilon_{570} \simeq 48{,}000\ M^{-1}\ cm^{-1}$) of rhodamine B,[10] the sample concentration (ranging from 10^{-6} to 10^{-3} M), and an estimated effective path length of 1 mm. Although this path length is not unreasonable, the need to estimate an effective path length to linearize the data is clearly not ideal for making quantitative measurements. It may be possible in the future to reduce this problem by more closely matching the focal length of the focusing lens and the width of the sample cell. In addition, it should be noted that knowledge of the path length is not required if one is willing to calibrate the system, which will be the case in future gas-phase studies.

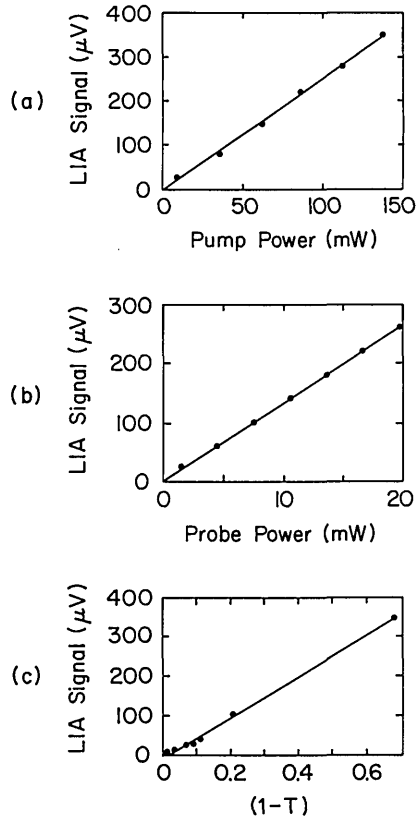

Fig. 5. Variation of the ASOPS signal with (a) pump power, (b) probe power, and (c) sample absorptance.

C. Spectra

Equation (7) was developed assuming that the probe beam stimulated emission only. However, the absorption and fluorescence bands of rhodamine B (see Fig. 4) overlap significantly in the wavelength region covered by current dye lasers. Since absorption of the probe follows the population of the ground state, which is clearly modulated at the same frequency as the excited-state population in this essentially two-level system, the observed signal will contain contributions from both absorption and stimulated emission.

To account for the effects of absorption, Eq. (1) is modified to

$$E_{pr}(t) \simeq E^0_{pr}[1 + \sigma_{em}bN_1(t) - \sigma_{ab}bN_0(t)], \quad (9)$$

where σ_{ab} is the cross section for absorption at the probe wavelength and N_0 is the number density of S_0. Assuming that the total number density N is distributed only in S_0 and S_1, then $N_0 = N - N_1$ at all times. Substituting this expression into Eq. (9) and rearranging yield

$$E_{pr}(t) = E^0_{pr}[1 - \sigma_{ab}bN + (\sigma_{em} + \sigma_{ab})bN_1(t)]. \quad (10)$$

Following the same reasoning used to derive Eq. (7) from Eq. (1) then leads to

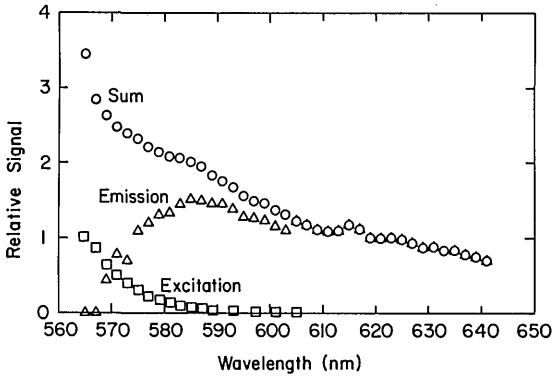

Fig. 6. Excitation, emission, and sum spectra of rhodamine B obtained by ASOPS.

$$V_{\mathrm{LIA}} \propto \left[\frac{\sigma_{\mathrm{em}} + \sigma_{\mathrm{ab}}}{h\nu_{\mathrm{pu}} A_{\mathrm{cs}}}\right] E^0_{\mathrm{pr}} E^0_{\mathrm{pu}} (1 - T)_{\mathrm{pu}}. \tag{11}$$

If the sample absorptance is small (i.e., <0.2), then $(1 - T)_{\mathrm{pu}} \simeq \sigma_{\mathrm{ab}} bN$, which on substitution into Eq. (11), followed by rearrangement, gives

$$V_{\mathrm{LIA}} \propto \left[\frac{E^0_{\mathrm{pr}} E^0_{\mathrm{pu}} bN\lambda_{\mathrm{pu}}}{hcA_{\mathrm{cs}}}\right] (\sigma^{\mathrm{pr}}_{\mathrm{em}} + \sigma^{\mathrm{pr}}_{\mathrm{ab}})\sigma^{\mathrm{pu}}_{\mathrm{ab}}, \tag{12}$$

where the superscripts pr and pu have been added to distinguish between cross sections at the pump and probe wavelengths, respectively, and ν_{pu} has been replaced by c/λ_{pu}.

In most pump/probe instruments a fixed pump wavelength is employed, and spectra are obtained by scanning the probe wavelength. According to Eq. (12), this procedure yields a sum spectrum related to both $\sigma^{\mathrm{pr}}_{\mathrm{em}}$ and $\sigma^{\mathrm{pr}}_{\mathrm{ab}}$. On the other hand, if the probe wavelength is fixed, scanning the pump wavelength yields an excitation spectrum related to $\sigma^{\mathrm{pu}}_{\mathrm{ab}}$. Hence, with appropriate scaling, one should be able to subtract the excitation spectrum from the sum spectrum with the difference being the emission spectrum.

Since we are primarily interested in the shape of the excitation and emission spectra rather than the absolute value of the cross sections, the sum data were first corrected for variations in laser power and normalized with respect to the corrected signal at λ'_{pr} (it is convenient to choose λ'_{pr} so that $\sigma^{\lambda'}_{\mathrm{ab}} = 0$) yielding

$$S^{\mathrm{sum}}_{\mathrm{norm}}(\lambda) = \frac{[V_{\mathrm{LIA}}/(E^0_{\mathrm{pr}}E^0_{\mathrm{pu}})](\lambda_{\mathrm{pr}})}{[V_{\mathrm{LIA}}/(E^0_{\mathrm{pr}}E^0_{\mathrm{pu}})](\lambda'_{\mathrm{pr}})} = \frac{\sigma^{\lambda}_{\mathrm{em}} + \sigma^{\lambda}_{\mathrm{ab}}}{\sigma^{\lambda'}_{\mathrm{em}}}. \tag{13}$$

Likewise, the excitation data were corrected for variations in laser power and pump wavelength and normalized with respect to the corrected signal at λ''_{pu} yielding

$$S^{\mathrm{ex}}_{\mathrm{norm}}(\lambda) = \frac{[V_{\mathrm{LIA}}/(E^0_{\mathrm{pr}}E^0_{\mathrm{pu}}\lambda)](\lambda_{\mathrm{pu}})}{[V_{\mathrm{LIA}}/(E^0_{\mathrm{pr}}E^0_{\mathrm{pu}}\lambda'')(\lambda''_{\mathrm{pu}})} = \frac{\sigma^{\lambda}_{\mathrm{ab}}}{\sigma^{\lambda''}_{\mathrm{ab}}}. \tag{14}$$

The normalized emission spectrum is then given by

$$S^{\mathrm{em}}_{norm}(\lambda) = S^{\mathrm{sum}}_{norm}(\lambda) - \frac{\sigma^{\lambda''}_{\mathrm{ab}}}{\sigma^{\lambda'}_{\mathrm{em}}} S^{\mathrm{ex}}_{norm}(\lambda) = \frac{\sigma^{\lambda}_{\mathrm{em}}}{\sigma^{\lambda'}_{\mathrm{em}}}, \tag{15}$$

which shows that if the appropriate scaling factor $\sigma^{\lambda''}_{\mathrm{ab}}/\sigma^{\lambda'}_{\mathrm{em}}$ is known, the emission spectrum can be calculated from the sum and excitation spectra.

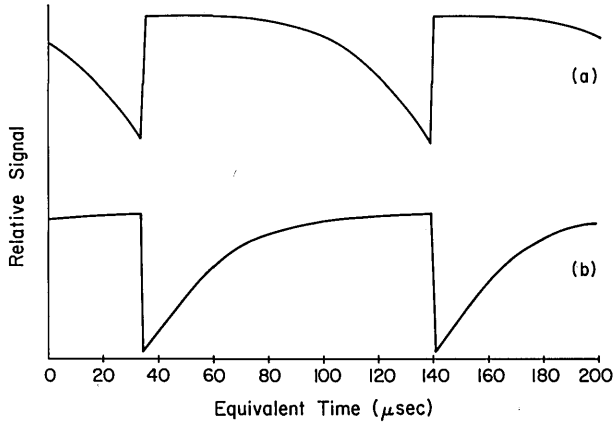

Fig. 7. Equivalent time decay of rhodamine B observed (a) on the pump beam and (b) on the probe beam. A smooth line has been drawn through the original data for presentation purposes.

Ideally, one would select λ'' so that $\sigma^{\lambda''}_{\mathrm{em}} = 0$; then $S^{\mathrm{sum}}_{\mathrm{norm}}(\lambda'')$ would be the desired scaling factor. Unfortunately, due to the limited tuning range of the dye lasers, this was not possible. However, if $\lambda''_{\mathrm{pr}} < \lambda_{\mathrm{pu}}$, then $S^{\mathrm{sum}}_{\mathrm{norm}}(\lambda'')$ can still be a reasonable estimate of the scaling factor if the probe beam now accesses a higher-energy transition than the pump beam, thus making it impossible to stimulate emission from the lowest vibrational level of S_1. The stimulated emission term in Eq. (9) would then depend not on N_1, but on N_1', the number density in the upper vibrational level accessed by the probe beam. Assuming that the two-level model holds (i.e., ignoring the Boltzmann distribution of states), $N_1' = 0$, and the stimulated emission term vanishes. Propagating this condition through to Eq. (13) gives $S^{\mathrm{sum}}_{\mathrm{norm}}(\lambda'') = \sigma^{\lambda''}_{\mathrm{ab}}/\sigma^{\lambda'}_{\mathrm{em}}$, which is the desired scaling factor.

Figure 6 shows the normalized sum and excitation spectra measured with the ASOPS instrument as well as the resulting emission spectrum calculated from Eq. (15). Although there are no sharp features against which to compare, the measured excitation and emission spectra follow the general trends observed in the known spectra (see Fig. 4).

D. Temporal studies

Equation (3) describes the probe–sample interaction as a function of the pump/probe temporal separation. As pointed out earlier, however, the ASOPS technique performs a time transformation of the decay. Hence the observed signal takes the same form as Eq. (3), but with the temporal parameters, t and τ, replaced by equivalent transformed parameters, t_{eq} and τ_{eq}, where the actual and equivalent parameters are related by

$$t_{\mathrm{eq}} = tf_{\mathrm{pu}}/(f_{\mathrm{pu}} - f_{\mathrm{pr}}). \tag{10}$$

Figure 7(a) shows the equivalent time decay of rhodamine B using a 570-nm pump beam and a 585-nm probe beam. The peak SNR was determined to be $\simeq$20. The repetition rate of the pump laser is 81.5970000 MHz, while that of the probe laser is

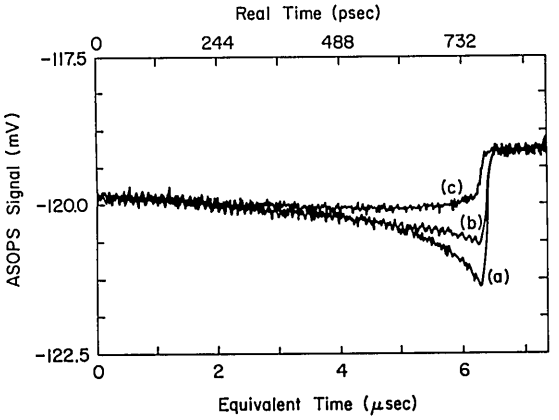

Fig. 8. Effect of polarization on the decay of rhodamine B. Polarization of the probe beam fixed (a) parallel, (b) at the magic angle, and (c) perpendicular to the polarization of the pump beam.

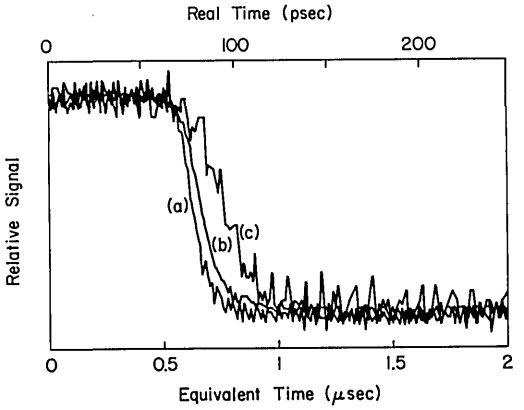

Fig. 9. Effect of frequency synthesizer stability of the decay of rhodamine B. Results for (a) phase-locked PTS, (b) free-running PTS, and (c) free-running Spectra-Physics frequency synthesizers.

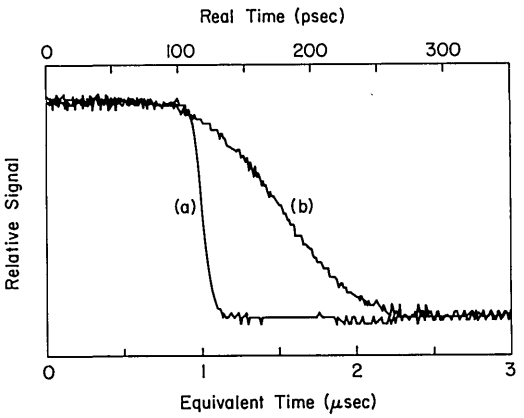

Fig. 10. Effect of trigger stability on the decay of rhodamine B where the trigger signal is derived (a) from the cross-correlation of the pump and probe beams and (b) from electronically mixed photodiode signals monitoring the two beams.

81.5870000 MHz, yielding a beat frequency of 10.0000 kHz. The measured lifetime of 18.6 μs, therefore, corresponds to an actual lifetime of 2.3 ns, which is in reasonable agreement with literature values[10,12] ranging from 2.3 to 3.2 ns. Since both the pump and probe beams lie in the absorption band of rhodamine B, the observed decay results from monitoring the recovery of the ground state. (Similar results have been observed when monitoring the excited state directly by stimulated emission.[3]) Since both beams excite the ground state, the role of the lasers is interchangeable, i.e., both beams modulate, at the beat frequency, the ground-state population seen by the other beam. Figure 7(b) shows the same experimental results as Fig. 7(a) but obtained by monitoring the pump beam rather than the probe beam. Since the period of the pump beam is shorter than that of the probe beam, each successive pump pulse samples the ground-state population at a slightly earlier time (relative to the probe pulse train) than its predecessor, while each successive probe pulse samples the ground-state population at a slightly later time (relative to the pump pulse train) than its predecessor. Hence, the decay in Fig. 7(b) is reversed in time relative to the decay in Fig. 7(a).

Due to the polarization of the pump and probe beams, the observed decay depends not only on the number densities in the states connected by the probe laser but also on rotation of the dipole moment of these populations with respect to the polarization of the probe beam. In liquids these rotations often occur on the picosecond time scale.[13,14] Closer examination of the leading edge of the rhodamine B decay, as shown in Fig. 8 where the polarization of the pump beam has been set parallel, perpendicular, and at the magic angle (55°) relative to the polarization of the probe beam, illustrates this effect and demonstrates the temporal capabilities of the ASOPS technique. As expected, the parallel arrangement exhibits a fast rise, while the perpendicular arrangement exhibits a slow rise relative to the magic angle configuration. All three decays eventually merge as a result of rotational randomization of the dipole moments. The rotational diffusion time of rhodamine B was determined to be 105 ps, which is in excellent agreement with the literature value of 102 ± 5 ps.[15]

The temporal response of the instrument is determined by (1) the stability of the beat frequency, (2) the stability of the trigger system, (3) the width of the pump and probe pulses, and (4) the magnitude of the beat frequency. Figure 9 shows the leading edge of the rhodamine B decay using three different schemes to generate the mode-locking frequencies. The schemes employ free-running and phase-locked frequency synthesizers from two different manufacturers. Not surprisingly, phase-locking the PTS frequency synthesizers (0.1-Hz resolution) yields the most stable beat frequency. Figure 10 shows the results obtained when using the two triggering schemes described earlier. The instability in the electronic scheme is probably caused by impedance mismatches between the various components and by intensity fluctuations in the lasers which cause jitter in the detection system.

The width of the pulses and the magnitude of the beat frequency are determined by the laser system and are factors over which we currently have little control. As mentioned earlier, the sampling interval and collec-

tion time are inversely related. This trade-off may in the future be minimized by operating the lasers at a higher repetition rate of 246 MHz (i.e., mode-locking the lasers on the third harmonic). For the same temporal resolution (1.5 ps), this higher repetition rate would decrease the collection time by a factor of 9. Conversely, the temporal resolution would increase by a factor of 9 for the same collection time (100 μs). The price in this case would be a decrease in the free temporal range from the current 12.2–4.1-ns.

The ultimate goal of this research is the development of the ASOPS technique as a combustion diagnostic in high-pressure flames. Future studies will, therefore, be directed toward applying this technique to combustion systems. After initial studies employing atomic sodium, we will investigate the hydroxyl radical as it is a major intermediate in flames and its spectroscopy is well known. The major difficulty anticipated is a significant drop in power and, therefore, signal, resulting from the need to frequency-double both dye lasers to access rotational transitions of the hydroxyl radical.

This Research was sponsored by the Air Force Office of Scientific Research, Air Force Systems Command, USAF under grant AFOSR-84-0323.

Yanan Jiang is a visiting professor on leave from Tsinghua University, Department of Precision Instruments, Beijing, China.

References

1. G. R. Fleming, "Applications of Continuously Operating, Synchronously Mode-Locked Lasers," Adv. Chem. Phys. **49**, 1 (1982).
2. F. E. Lytle, R. M. Parrish, and W. T. Barnes, "An Introduction to Time-Resolved Pump/Probe Spectroscopy," Appl. Spectrosc. **39**, 444 (1985).
3. P. A. Elzinga, F. E. Lytle, Y. Jiang, G. B. King, and N. M. Laurendeau, "Pump/Probe Spectroscopy by Asynchronous Optical Sampling," Appl. Spectrosc. **41**, 2 (1987).
4. G. J. Blanchard and M. J. Wirth, "Measurement of Small Absorbances by Picosecond Pump–Probe Spectroscopy," Anal. Chem. **58**, 532 (1986).
5. P. Bado, S. B. Wilson, and K. R. Wilson, "Multiple Modulation for Optical Pump–Probe Spectroscopy," Rev. Sci. Instrum. **53**, 706 (1982).
6. E. L. Quitevis, E. F. Gudgin Templeton, and G. A. Kenney-Wallace, "Multiple Modulation Spectroscopy at Radiofrequencies for Picosecond Spectroscopy," Appl. Opt. **24**, 318 (1985).
7. L. Andor, A. Lorincz, J. Siemion, D. D. Smith, and S. A. Rice, "Shot-Noise-Limited Detection Scheme for Two-Beam Laser Spectroscopies," Rev. Sci. Instrum. **55**, 64 (1984).
8. A. J. Alfano, F. K. Fong, and F. E. Lytle, "High Repetition Rate Subnanosecond Gated Photon Counting," Rev. Sci. Instrum. **54**, 967 (1983).
9. T. Kanada and D. L. Franzen, "Optical Waveform Measurement by Optical Sampling with a Mode-Locked Laser Diode," Opt. Lett. **11**, 4 (1986).
10. I. B. Berlman, *Handbook of Fluorescence Spectra of Aromatic Molecules* (Academic, New York, 1971), Graph 205A.
11. P. A. Elzinga, "Asynchronous Optical Sampling," M. S. Thesis, Purdue U., West Lafayette, IN (Dec. 1986).
12. H. R. Stadelmann, "Measurement of the Fluorescence Decay Times of some Organic Dyes," J. Luminesc. **3**, 143 (1970).
13. T. J. Chuang and K. B. Eisenthal, "Studies of Effects of Hydrogen Bonding on Orientational Relaxation using Picosecond Light Pulses," Chem. Phys. Lett. **11**, 368 (1971).
14. C. V. Shank and E. P. Ippen, "Anisotropic Absorption Saturation with Picosecond Pulses," Appl. Phys. Lett. **26**, 62 (1975).
15. K. Berndt, H. Durr, and D. Palme, "Picosecond Phase Fluorometry by Mode-Locked CW Lasers," Opt. Commun. **42**, 419 (1982).